ACS APPLIED MATERIALS & INTERFACES

Research Article

www.acsami.org

pn-Heterojunction Effects of Perylene Tetracarboxylic Diimide Derivatives on Pentacene Field-Effect Transistor

Seong Hun Yu,[†] Boseok Kang,[§] Gukil An,[∥] BongSoo Kim,[⊥,#,▽] Moo Hyung Lee,[○] Moon Sung Kang,[○] Hyunjung Kim,[∥] Jung Heon Lee,[‡] Shichoon Lee,[¶] Kilwon Cho,[§] Jun Young Lee,*[,†] and Jeong Ho Cho*[,†,‡]

[†]Department of Chemical Engineering and [‡]SKKU Advanced Institute of Nanotechnology (SAINT), Sungkyunkwan University, Suwon, 440-746, Korea

[§]Department of Chemical Engineering, Pohang University of Science and Technology, Pohang, 790-784, Korea

[∥]Department of Physics, Sogang University, Seoul, 121-742, Korea

[⊥]Photo-electronic Hybrids Research Center, Korea Institute of Science and Technology (KIST), Seoul, 136-791, Korea

[#]Green School (Graduate School of Energy and Environment) and [▽]Nanomaterials Science and Engineering, Korea University of Science & Technology, Daejeon, 305-350, Korea

[○]Department of Chemical Engineering, Soongsil University, Seoul, 156-743, Korea

[¶]Department of Materials Science and Engineering, Jungwon University, Goesan 367-805, Korea

Supporting Information

ABSTRACT: We investigated the heterojunction effects of perylene tetracarboxylic diimide (PTCDI) derivatives on the pentacene-based field-effect transistors (FETs). Three PTCDI derivatives with different substituents were deposited onto pentacene layers and served as charge transfer dopants. The deposited PTCDI layer, which had a nominal thickness of a few layers, formed discontinuous patches on the pentacene layers and dramatically enhanced the hole mobility in the pentacene FET. Among the three PTCDI molecules tested, the octyl-substituted PTCDI, PTCDI-C_8, provided the most efficient hole-doping characteristics (p-type) relative to the fluorophenyl-substituted PTCDIs, 4-FPEPTC and 2,4-FPEPTC. The organic heterojunction and doping characteristics were systematically investigated using atomic force microscopy, 2D grazing incidence X-ray diffraction studies, and ultraviolet photoelectron spectroscopy. PTCDI-C_8, bearing octyl substituents, grew laterally on the pentacene layer (2D growth), whereas 2,4-FPEPTC, with fluorophenyl substituents, underwent 3D growth. The different growth modes resulted in different contact areas and relative orientations between the pentacene and PTCDI molecules, which significantly affected the doping efficiency of the deposited adlayer. The differences between the growth modes and the thin-film microstructures in the different PTCDI patches were attributed to a mismatch between the surface energies of the patches and the underlying pentacene layer. The film-morphology-dependent doping effects observed here offer practical guidelines for achieving more effective charge transfer doping in thin-film transistors.

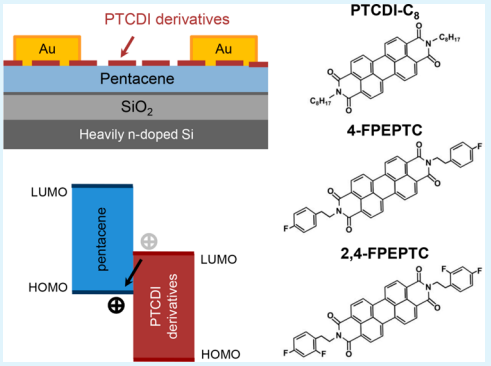

KEYWORDS: *pn-heterojunction, charge transfer doping, organic field-effect transistor, perylene tetracarboxylic diimide, pentacene*

1. INTRODUCTION

Organic field-effect transistors (OFETs) have developed rapidly over the last few decades due to their wide range of potential applications in flexible display drivers, radio frequency identification tags (RFIDs), and sensors.[1−9] The considerable efforts in this field have achieved outstanding improvements in OFET performances. Such efforts include the synthesis of new electronic components (conducting, semiconducting, and dielectric materials), the development of novel device structures, and the introduction of a variety of thin-film processing techniques.[10−23] OFETs exhibiting carrier mobilities comparable to those of amorphous silicon field-effect transistors (FETs) [>1 $cm^2/(V\ s)$] were recently reported.[24−26] In most cases, the mobility and threshold voltage of OFETs must be further improved to serve the requirement of high-performance electronic devices.

OFET performances may be further improved using n-type semiconductor patches that partially cover a p-type semiconducting channel.[27−30] These pn-heterostructures with suitable energy level alignment can transfer electrons in a p-type channel to an n-type semiconductor patch, or holes can migrate from the patches to the p-type channel. Charge transfer

Received: November 10, 2014
Accepted: January 12, 2015
Published: January 12, 2015

DOI: 10.1021/am507854s
ACS Appl. Mater. Interfaces 2015, 7, 2025−2031

between the molecules can dramatically enhance the carrier mobility of a device. These effects may be obtained by positioning the lowest unoccupied molecular orbital (LUMO) level of an n-type patch near the highest occupied molecular orbital (HOMO) level of a p-type channel. Beyond the energy alignment issue, the crystalline microstructure as well as the film morphology of an n-type material grown on a p-type layer must be considered to induce efficient charge transfer at the interface. Until now, however, these effects have not been addressed in detail.

In this study, we investigated the heterojunction effects of three different n-type PTCDI derivatives (PTCDI-C_8, 4-FPEPTC, and 2,4-FPEPTC) on the pentacene OFET once the derivatives are attached as patches. The PTCDI derivatives are representative n-type semiconducting materials with high electron mobilities that provide favorable energy alignment for charge transfer at the interface with pentacene.[31−34] The three PTCDI derivatives include different substituents on the nitrogen atoms of the imide groups, i.e., octyl, (4-fluorophenyl)ethyl, and (2,4-fluorophenyl)ethyl. The molecules with different fluorine group contents were expected to exhibit different interactions with the underlying pentacene layer, especially as the PTCDI derivatives tended to stand upright on pentacene in an edge-on configuration.[30,35,36] The HOMO/LUMO energy levels and band gaps of these PTCDI derivatives were nearly identical (Figure 1). Accordingly, they can serve as

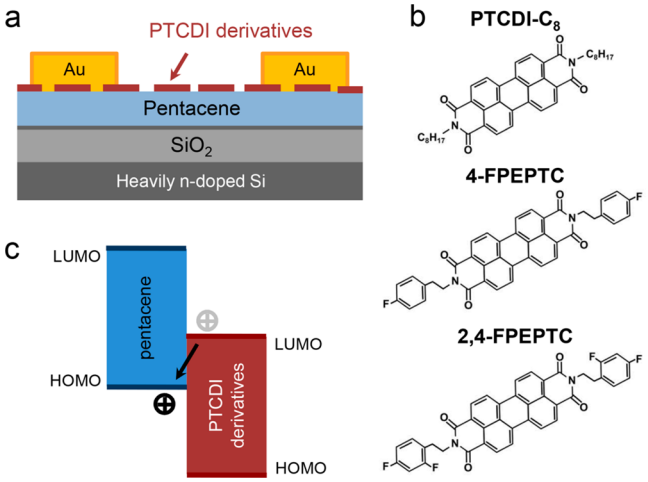

Figure 1. (a) Schematic cross section of the pentacene OFET with discontinuous n-type PTCDI derivative patches. (b) Chemical structures of PTCDI derivatives (PTCDI-C_8, 4-FPEPTC, and 2,4-FPEPTC) used in this study. (c) Energy level diagram for pentacene−PTCDI system.

model systems for investigating the impact of the charge transfer patch microstructure while energy alignment issues are avoided. The electrical properties of the OFETs (carrier mobility, threshold voltage, and activation energy for charge carrier hopping) were measured while controlling the density and thickness of the n-type patches on the pentacene layers. The PTCDI-C_8 patches exhibited p-type doping effects that were more efficient than those obtained using 4-FPEPTC and 2,4-FPEPTC. These differences were investigated systematically using atomic force microscopy (AFM), 2D grazing incidence X-ray diffraction (GIXD), and ultraviolet photoelectron spectroscopy (UPS). We attributed the different crystalline microstructures and film morphologies of the n-type patches on pentacene layers to the surface energy mismatch between the n-type patches and the pentacene film.

2. EXPERIMENTAL SECTION

Device Fabrication. The OFETs were fabricated on a heavily n-doped Si wafer substrate bearing a thermally grown 300-nm-thick SiO_2 layer. The Si wafer was cleaned by sequential sonication for 10 min in each of acetone, 2-propanol, and distilled water. The substrate was then dried in a vacuum oven. A 7-nm-thick pentacene (Sigma-Aldrich, 99%) film was thermally deposited onto the SiO_2 gate dielectric to form a p-channel semiconductor at a rate of 0.2 Å/s under vacuum (5.0×10^{-6} Torr). The doping layers were prepared by subsequently depositing *N*,*N*′-dioctyl-3,4,9,10-perylene tetracarboxylic diimide (PTCDI-C_8) (Sigma-Aldrich, 98%), *N*,*N*′-bis[2-(4-fluorophenyl)-ethyl]-3,4,9,10-perylene tetracarboxylic diimide (4-FPEPTC) (Lumtec, sublimed grade), or *N*,*N*′-bis[2-(2,4-difluorophenyl)ethyl]-3,4,9,10-perylene tetracarboxylic diimide (2,4-FPEPTC) (Lumtec, sublimed grade) to various thicknesses onto the pentacene thin film without breaking the vacuum in the evaporation chamber. The thicknesses of the organic semiconductor layers were monitored using a quartz crystal microbalance (QCM). Finally, a 40-nm-thick Au layer was thermally deposited through a shadow mask to form source−drain electrodes with a channel length (L) and width (W) of 50 and 1000 μm, respectively.

Measurements. The electrical characteristics of the OFETs were measured under vacuum (<10^{-3} Torr) using a Janis cryogenic probe-station connected to Keithley 2400 and 236 source/measure units. The temperature-dependent mobility measurements were conducted by introducing liquid nitrogen into the cryogenic probe station system. The surface morphologies of the pentacene films prepared with PTCDI derivative nanopatches were investigated using multimode atomic force microscopy (AFM) in the tapping mode (Nanoscope IIIA). The 2D GIXD studies were performed at the 3C and 9A beamlines of the Pohang Light Source II, Pohang, Korea. UPS measurements were carried out using a He I (21.2 eV) discharge lamp in an AXIS-NOVA system (Kratos Inc.) under high vacuum (~10^{-9} Torr). A sample bias of −9 V was used to separate the sample from the secondary edge for analysis.

3. RESULTS AND DISCUSSION

Figure 1a shows a schematic cross-sectional diagram of the pentacene FETs prepared with the n-type PTCDI derivatives. Three different PTCDI derivatives of PTCDI-C_8, 4-FPEPTC, and 2,4-FPEPTC (Figure 1b) with various thicknesses were thermally deposited onto the pentacene layer. The HOMO/LUMO energy levels and band gaps were nearly identical (Supporting Information, Figure S1), although the derivatives included different substituents on the nitrogen atoms of the imide groups [octyl, (4-fluorophenyl)ethyl, and (2,4-difluorophenyl)ethyl]. The PTCDI patches induced hole transfer from the PTCDI LUMO to the pentacene HOMO via suitable energy alignment.[29,30] The energy level diagram of a typical p-doping mechanism in a pn-heterostructure is illustrated in Figure 1c.

Figures 2a and S2 (Supporting Information) show the representative transfer characteristics [drain current (I_D)−gate voltage (V_G)] of the OFETs based on a 7-nm-thick pentacene channel prepared with n-type PTCDI-C_8, 4-FPEPTC, and 2,4-FPEPTC patches. Generally, the overlying patch-type charge transfer doping layers can affect the underneath active channel only down to a finite depth. Therefore, the thin pentacene layer with a thickness of 7 nm was utilized to verify the surface transfer doping effect more obviously. The devices exhibited typical p-channel behavior (i.e., I_D increased as V_G decreased), and I_D increased gradually with the nominal deposition thickness of the n-type patches. Below a critical thickness, the

DOI: 10.1021/am507854s
ACS Appl. Mater. Interfaces 2015, 7, 2025−2031

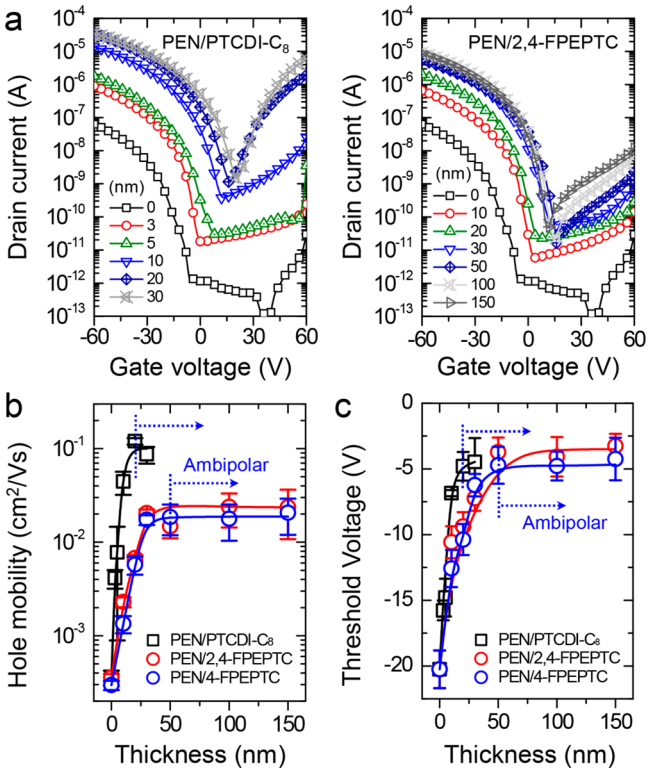

Figure 2. (a) Representative transfer characteristics of the pentacene OFETs based on PTCDI-C_8 and 2,4-FPEPTC patches with different thicknesses (V_D = −40 V). (b) Hole mobility and (c) threshold voltage of the pentacene OFETs based on n-type PTCDI-C_8, 4-FPEPTC, and 2,4-FPEPTC patches with varying film thicknesses.

PTCDI patches remained unconnected, and electron transport did not occur in the channel. By contrast, the deposition of a sufficient PTCDI layer provided a pathway for electron transport, and ambipolar charge transport was favored. The critical thickness required for conversion from p-channel to ambipolar transport was only 10 nm for PTCDI-C_8, whereas both 4-FPEPTC and 2,4-FPEPTC required much higher critical thicknesses of around 50 nm.

The heterojunction effects were investigated quantitatively by monitoring the mobility enhancement and threshold voltage shift in the pentacene FETs while varying the thickness of the n-type patches. The hole mobility in the saturation regime and the threshold voltage were extracted from the slope and x-intercept of the transfer curve, which was plotted as $I_D^{1/2}$ versus V_G, using a transistor equation typical of the saturation regime: $I_D = \mu C_i W/2L(V_G - V_{th})^2$, where L and W are the channel length and width, μ is the hole mobility, and C_i is the specific capacitance of the gate dielectric. Figure 2b,c summarizes the average hole mobility (μ) and threshold voltage (V_{th}) as a function of the PTCDI-C_8 (black), 2,4-FPEPTC (red), or 4-FPEPTC (blue) layer thickness deposited on the pentacene channel layer. As the patch thickness increased, the hole mobility initially increased dramatically but then become saturated beyond a certain thickness. For example, the hole mobilities of the pentacene OFETs increased from 3.6×10^{-4} (pristine) to 0.12 $cm^2/(V\ s)$ (30-nm-thick PTCDI-C_8 patches), whereas both the 4-FPEPTC and 2,4-FPEPTC OFETs yielded a mobility of only 0.02 $cm^2/(V\ s)$ at the same deposition thickness. This mobility enhancement was attributed to the interfacial hole transfer between the penatacene HOMO (−4.9 eV) and overlying n-type patch LUMO (−4.3 eV), leading to the filling of localized traps in the pentacene layer. In addition, the on/off current ratios below the critical thickness are summarized in Figure S3 (Supporting Information).

Although the positions of the HOMO levels were nearly the same in the different patch materials, yielding similar energy alignment with the pentacene energy levels, the pn-heterojunction effects differed (a 300-fold mobility increase was observed for the PTCDI-C_8 patch system and a 50-fold mobility increase was observed for the 4-FPEPTC and 2,4-FPEPTC patch systems). This result was attributed to the crystalline microstructures and film morphologies of the different n-type patches (as discussed below). The threshold voltage shifted toward positive values as the n-type patch thickness increased, providing direct evidence for the p-type doping of pentacene.[37−39] The threshold-voltage shift followed a trend similar to that observed in the measured mobilities as a function of the patch thickness. Beyond a critical thickness value, the mobility and threshold voltage shifts reached saturation. The resulting devices showed ambipolar characteristics once the electron-transport pathways were connected. Because the electrical characteristics of the FETs prepared with 4-FPEPTC and 2,4-FPEPTC patches exhibited no substantial performance differences, subsequent experiments focused on comparing the impacts of the PTCDI-C_8 and 2,4-FPEPTC patches.

The trap-filling effects resulting from hole transfer by the n-type patches were investigated by measuring the temperature-dependent transistor properties over the range 77−300 K. The hole mobilities were extracted from the transfer curves measured at different temperatures. As shown in Figure 3, all devices exhibited a decrease in the hole mobility as the temperature decreased, providing a clear linear relationship in the Arrhenius plot of ln μ vs $1/k_BT$, where k_B is Boltzmann's constant. The thermal activation energy (E_A) for carrier hopping in the pentacene OFETs prepared with n-type patches

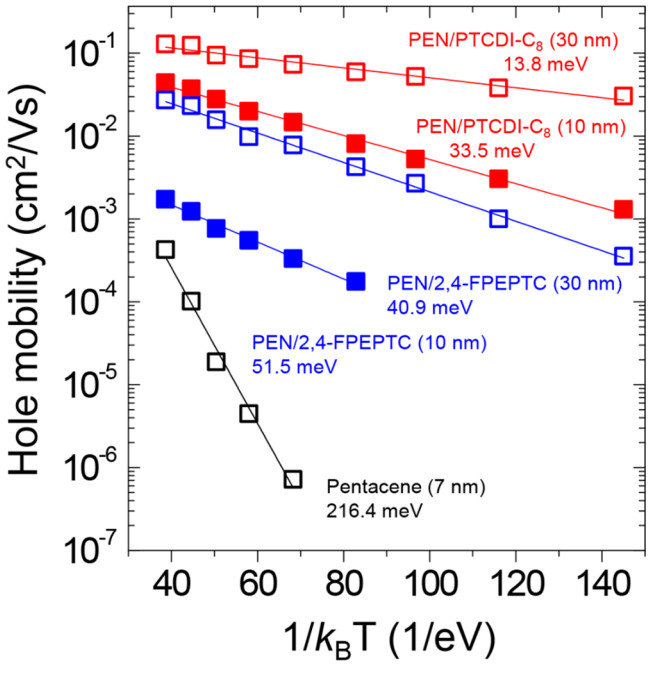

Figure 3. Arrhenius plot of hole mobility for the pentacene OTFTs based on n-type PTCDI-C_8 and 2,4-FPEPTC patches.

DOI: 10.1021/am507854s
ACS Appl. Mater. Interfaces 2015, 7, 2025−2031

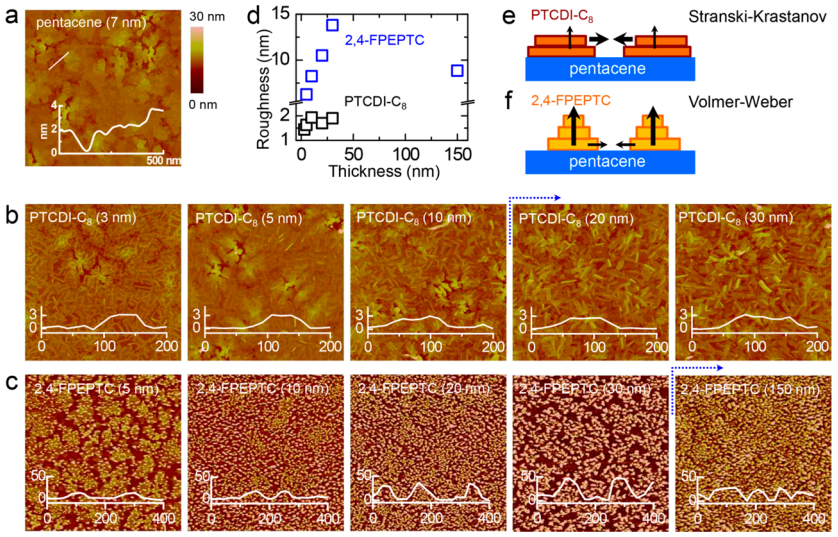

Figure 4. (a) AFM image of 7-nm-thick pentacene films. AFM images of 7-nm-thick pentacene films partially covered with (b) PTCDI-C_8 and (c) 2,4-FPEPTC. The insets show the cross-sectional height profile of n-type patches with increasing thicknesses. (d) RMS roughness of 7-nm-thick pentacene films partially covered with PTCDI-C_8 and 2,4-FPEPTC. Growth modes of two types of n-type (e) PTCDI-C_8 and (f) 2,4-FPEPTC patches. Black arrows indicate the growth direction of n-type patches.

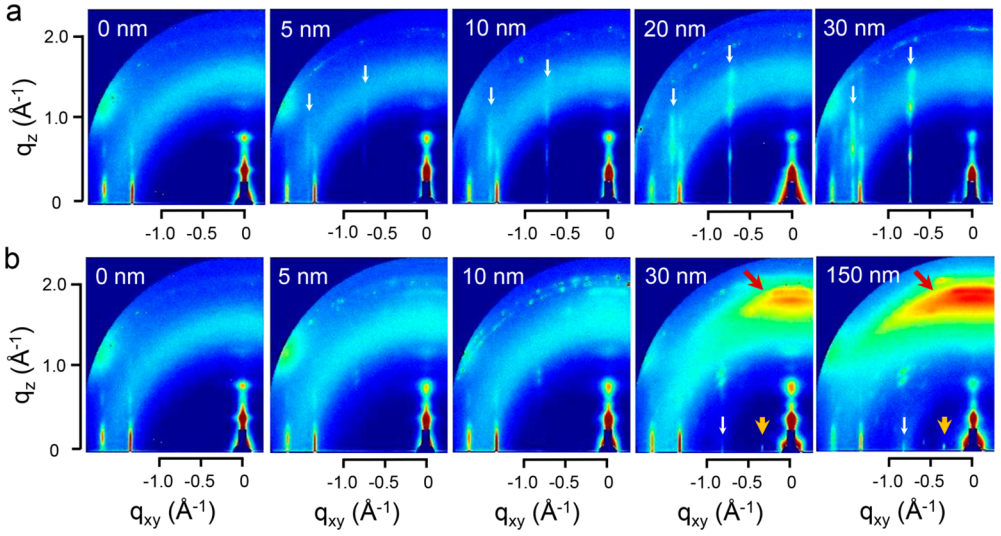

Figure 5. 2D grazing incidence X-ray diffraction (GIXD) pattern for pentacene films with n-type patches of (a) PTCDI-C_8 and (b) 2,4-FPEPTC molecules with increasing deposition thicknesses.

could be extracted using the following equation: $\mu = \mu_0 \exp[-E_A/k_BT]$, where μ_0 is the free carrier mobility. Thermally activated transport in organic semiconductors can be described using a multiple trapping and release (MTR) model.[40,41] The activation energy indicates the energy needed for charge carriers to escape from the trap sites and reach the transport level.[42] The activation energies extracted from the pentacene OFETs prepared with PTCDI-C_8 and 2,4-FPEPTC patches are shown in Figure 3. Compared with the E_A values obtained from pristine pentacene (216.4 meV), the pentacene devices prepared with 10-nm-thick PTCDI-C_8 or 2,4-FPEPTC patches exhibited much smaller E_A values of 33.5 and 51.5 meV, respectively. These results demonstrated that the overlying n-type patches effectively reduce the traps depths, as a result of filling the deep traps with holes transferred from the n-type patches. The thicker doping layers formed by the PTCDI-C_8 and 2,4-FPEPTC reduced the activation energy in the both cases. The E_A values of the PTCDI-C_8 OFETs were smaller than obtained from the 2,4-FPEPTC devices, even at a given deposition thickness of 10 or 30 nm, indicating that the PTCDI-C_8 patches contributed more effectively to charge transfer and deep-trap filling, as compared with the 2,4-FPEPTC patches.

The n-type patches affected the OFET performances to different degrees. These effects could be understood in terms of the crystalline nanostructures and film morphologies of the n-type patches on the pentacene layer. These properties were investigated using AFM and 2D GIXD. The film morphologies of the pentacene films prepared with two types of n-type patches were first characterized using AFM. Figure 4a shows an AFM image obtained from a 7-nm-thick pentacene film with faceted terrace-like layered structures.[43,44] As the PTCDI-C_8 molecules were deposited onto the pentacene layer (Figure 4b), the PTCDI-C_8 patches formed a rod-shaped morphology and were uniformly distributed over the pentacene film. The rods grew laterally as the PTCDI-C_8 deposition thickness

DOI: 10.1021/am507854s
ACS Appl. Mater. Interfaces 2015, 7, 2025−2031

increased.[30] The insets reveal that the height profiles of the PTCDI-C_8 rods remained constant, regardless of the deposition thickness, indicating that 3D island growth was not preferred for PTCDI-C_8. This type of growth is described as the Stranski–Krastanov growth mode (Figure 4e). This growth mode arises because the deposited molecules are more strongly attracted to the pentacene than to each other due to the well-matched surface energies of the deposited film and the pentacene layer or the favorable interactions between the alkyl groups in PTCDI-C_8 and the benzene groups in pentacene.[45] The deposition of PTCDI-C_8 patches to thicknesses exceeding 20 nm produces a continuous network of the PTCDI-C_8 rods. This thickness corresponds to the transition point between p-channel behavior to ambipolar FET operation, as shown in Figure 2.

The 2,4-FPEPTC islands grew vertically rather than laterally on the pentacene layer, and the island height increased to 50 nm as the deposition thickness increased to 30 nm (Figure 4c). This behavior may result from the surface energy mismatch between the 2,4-FPEPTC patches containing fluorine groups and the underlying pentacene films with aromatic rings. This 3D island growth is known as the Volmer–Weber growth (VW) growth mode (Figure 4f).[46] Beyond a nominal thickness of 30 nm, the 2,4-FPEPTC islands merged with one another at their bases, which reduced variations in the height profile across the islands (as observed in the AFM images). The surface roughness at 150 nm thick was, therefore, low (Figure 4d). By contrast, the film surface roughness did not change significantly during the deposition of PTCDI-C_8 patches due to the Stranski–Krastanov growth mode, as shown in Figure 4d. The 3D island growth in the 2,4-FPEPTC patches did not increase the areal coverage with respect to the bottom pentacene layer, which decreased the charge transfer efficiency between the semiconducting layers.

The microstructural characteristics of the PTCDI-C_8 and 2,4-FPEPTC patches on a pentacene layer were corroborated by collecting 2D GIXD measurements on films of various deposition thicknesses (Figure 5). In the absence of the patches, a pristine 7-nm-thick pentacene film displayed intense (00l) crystalline reflections along the q_z direction (surface normal), indicating that the pentacene layer grew in a "thin-film" crystalline phase on the SiO_2/Si substrates. Furthermore, the {1, ±1} and {0, 2} reflections at q_{xy} = 1.35 and 1.67 Å^{-1} appeared to be oriented vertically with respect to the given q_{xy} direction (Figure 6, black lines). These vertically aligned Bragg rod reflections indicated that the pentacene molecules were directed toward the surface normal and were highly ordered along the in-plane direction.[43,45] As the patch molecules were deposited, additional peaks appeared in the pentacene reflection pattern. The PTCDI-C_8 patches on the pentacene layer yielded two new Bragg rod peaks at q_{xy} = ∼0.75 and ∼1.41 Å^{-1}. These peaks gradually increased in intensity as the deposition thickness increased (Figures 5a and 6). These peaks correspond to the {±1, 0} and {0, ±1} reflections of PTCDI-C_8, respectively, indicating that the PTCDI-C_8 molecules adopted a standing-up orientation (i.e., the a–b plane was parallel to the pentacene surface) and formed a laterally well-ordered structure.[35] The intensities of the Bragg rod peaks increased with the PTCDI-C_8 deposition thickness, providing evidence for the 2D growth of the PTCDI-C_8 patches on pentacene (see the Supporting Information, Figure S4). In striking contrast to PTCDI-C_8, additional peaks along the q_z direction were observed in the GIXD patterns collected from the 2,4-FPEPTC patches. These peaks were likely due to the 3D growth of the 2,4-FPEPTC structures. The multiple peaks (red arrows in Figure 5b) may indicate the presence of lying-down crystalline domains (i.e., the a–c plane was parallel to the pentacene surface).[25,47] This conjecture was supported by the fact that the weak peaks along the in-plane direction (yellow arrows in Figure 5b) corresponded to a length of ∼17.5 Å, which was slightly smaller than the c-axis length (∼19.7 Å) in the PTCDI-C_8 unit cell. The long-axis length of the 2,4-FPEPTC molecules was slightly shorter than the length of the PTCDI-C_8 molecules. The standing-up crystalline domains were also observed among 2,4-FPEPTC patches with a deposition thickness exceeding 30 nm, as indicated by the peaks present at q_{xy} = ∼0.85 Å in the in-plane direction (white arrows in Figure 5b). These results suggested that, unlike the homogeneously grown PTCDI-C_8 crystallites, the differently oriented crystallites might be randomly distributed in the 2,4-FPEPTC thin films.

Parts a and b of Figure 7 show the ultraviolet photoemission spectroscopy (UPS) spectra obtained from the pentacene films prepared with n-type PTCDI-C_8 or 2,4-FPEPTC patches, respectively, at the secondary electron cutoff and HOMO

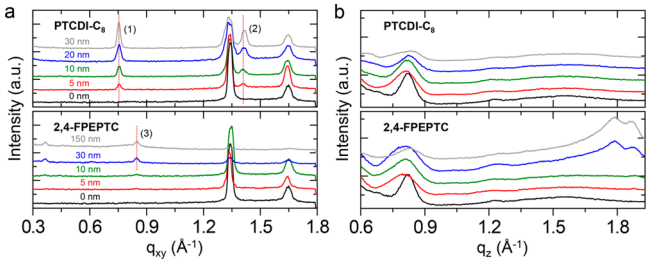

Figure 6. (a) In-plane and (b) out-of-plane profiles of the pentacene films with n-type PTCDI-C_8 and 2,4-FPEPTC patches as a function of the deposition thickness. These profiles were extracted from Figure 5

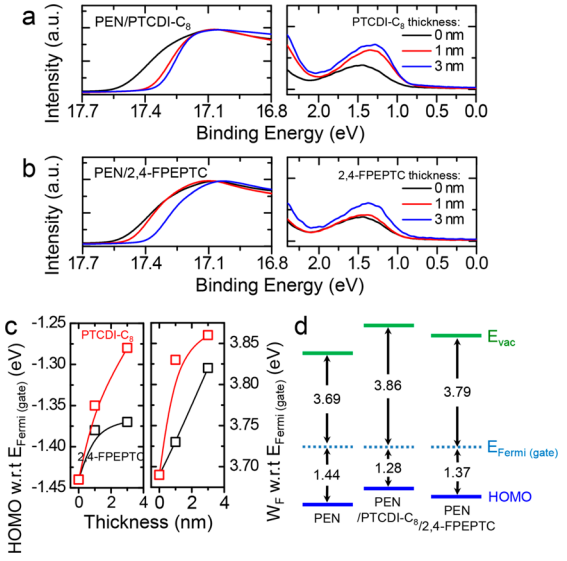

Figure 7. UPS spectra of the pentacene films with the n-type (a) PTCDI-C_8 and (b) 2,4-FPEPTC patches. (c) HOMO levels and work function (WF) as a function of the thicknesses of n-type patches. (d) Schematic band structures of the pristine pentacene and pentacene with n-type PTCDI-C_8 and 2,4-FPEPTC patches (3 nm deposition thickness).

DOI: 10.1021/am507854s
ACS Appl. Mater. Interfaces 2015, 7, 2025–2031

regions of pentacene for various n-type patches thicknesses. As the n-type molecules were deposited onto the pentacene layer, the HOMO levels of the pentacene shifted slightly toward lower binding energies in both cases. The HOMO states shifted with respect to the Fermi level of the gate electrode, indicating that p-type doping occurred.[37,39] Further increases in the doping thickness led to additional shifts in the Fermi level, generating additional free holes. The ionization potentials remained nearly constant. The HOMO level and work function shifted depending on the n-type patch thickness, as summarized in Figure 7c,d. The PTCDI-C_8 patches induced greater p-doping effects on the pentacene film compared to the 2,4-FPEPTC patches. These results were consistent with the observed threshold voltage shift described above (Figure 2). The agreement between the UPS data and the OFET properties reflected the fact that the patches effectively doped the pentacene molecules in the channel region.

4. CONCLUSION

In conclusion, we investigated the microstructures of three different PTCDI derivatives and characterized the resulting pn-heterojunction effects on the pentacene films. The interactions between the patch molecules and underlying pentacene film, along with the surface energy mismatch, induced these molecules to assemble via distinct growth modes on the pentacene layer. Two-dimensional growth was observed among the PTCDI-C_8 patches, and 3D growth was observed among the 2,4-FPEPTC patches. The favored growth mode for PTCDI-C_8 enlarged the areal coverage on the pentacene layer for a given nominal thickness compared to the areal coverage obtained from the other molecules. The use of PTCDI-C_8 patches on pentacene enhanced the hole mobility by a factor of 300 compared to the corresponding value measured in a reference pristine pentacene film. By contrast, the 2,4-FPEPTC patches provided only a 40-fold increase in the mobility. These results provide important background information that can guide the utilization of pn-heterojunction patches in OFET research.

■ ASSOCIATED CONTENT

Supporting Information

The UPS and UV absorption spectra of the PTCDI-C_8 and 2,4-FPEPTC films; transfer characteristics of the pentacene OFETs with 4-FPEPTC patches; on/off current ratio of the pentacene OFETs based on the n-type PTCDI-C_8, 4-FPEPTC, and 2,4-FPEPTC patches with different thicknesses; and intensities of the XRD in-plane peaks of the PTCDI-C_8 and 2,4-FPEPTC patches deposited onto pentacene layer as a function of the deposition thickness. This material is available free of charge via the Internet at http://pubs.acs.org.

■ AUTHOR INFORMATION

Corresponding Authors

*J.Y.L. e-mail: jylee7@skku.edu.
*J.H.C. e-mail: jhcho94@skku.edu.

Author Contributions

The manuscript was written through contributions of all authors.

Notes

The authors declare no competing financial interest.

■ ACKNOWLEDGMENTS

This research was supported by Basic Science Research Program through the National Research Foundation of Korea (NRF) funded by the Ministry of Science, ICT & Future Planning (2013R1A2A2A01015700, 2013R1A1A2011897, and 2009-0083540).

■ REFERENCES

(1) Park, Y. M.; Desai, A.; Salleo, A.; Jimison, L. Solution-Processable Zirconium Oxide Gate Dielectrics for Flexible Organic Field Effect Transistors Operated at Low Voltages. *Chem. Mater.* **2013**, *25*, 2571−2579.
(2) Peng, B.; Ren, X.; Wang, Z.; Wang, X.; Roberts, R. C.; Chan, P. K. L. High Performance Organic Transistor Active-Matrix Driver Developed on Paper Substrate. *Sci. Rep.* **2014**, *4*, 6430.
(3) Gelinck, G. H.; Huitema, H. E. A.; van Veenendaal, E.; Cantatore, E.; Schrijnemakers, L.; van der Putten, J. B. P. H.; Geuns, T. C. T.; Beenhakkers, M.; Giesbers, J. B.; Huisman, B.-H.; Meijer, E. J.; Benito, E. M.; Touwslager, F. J.; Marsman, A. W.; van Rens, B. J. E.; de Leeuw, D. M. Flexible Active-Matrix Displays and Shift Registers Based on Solution-Processed Organic Transistors. *Nat. Mater.* **2004**, *3*, 106−110.
(4) Baude, P. F.; Ender, D. A.; Haase, M. A.; Kelley, T. W.; Muyres, D. V.; Theiss, S. D. Pentacene-Based Radio-Frequency Identification Circuitry. *Appl. Phys. Lett.* **2003**, *82*, 3964−3966.
(5) Subramanian, V.; Fréchet, J. M.; Chang, P. C.; Huang, D. C.; Lee, J. B.; Molesa, S. E.; Murphy, A. R.; Redinger, D. R.; Volkman, S. K. Progress toward Development of All-Printed RFID Tags: Materials, Processes, and Devices. *Proc. IEEE* **2005**, *93*, 1330−1338.
(6) Lipomi, D. J.; Vosgueritchian, M.; Tee, B. C. K.; Hellstrom, S. L.; Lee, J. A.; Fox, C. H.; Bao, Z. Skin-Like Pressure and Strain Sensors Based on Transparent Elastic Films of Carbon Nanotubes. *Nat. Nanotechnol.* **2011**, *6*, 788−792.
(7) Takei, K.; Takahashi, T.; Ho, J. C.; Ko, H.; Gillies, A. G.; Leu, P. W.; Fearing, R. S.; Javey, A. Nanowire Active-Matrix Circuitry for Low-Voltage Macroscale Artificial Skin. *Nat. Mater.* **2010**, *9*, 821−826.
(8) Verploegen, E.; Sokolov, A. N.; Akgun, B.; Satija, S. K.; Wei, P.; Kim, D.; Kapelewski, M. T.; Bao, Z.; Toney, M. F. Swelling of Polymer Dielectric Thin Films for Organic-Transistor-Based Aqueous Sensing Applications. *Chem. Mater.* **2013**, *25*, 5018−5022.
(9) Janata, J.; Josowicz, M. Conducting Polymers in Electronic Chemical Sensors. *Nat. Mater.* **2003**, *2*, 19−24.
(10) Shinamura, S.; Osaka, I.; Miyazaki, E.; Nakao, A.; Yamagishi, M.; Takeya, J.; Takimiya, K. Linear- and Angular-Shaped Naphthodithiophenes: Selective Synthesis, Properties, and Application to Organic Field-Effect Transistors. *J. Am. Chem. Soc.* **2011**, *133*, 5024−5035.
(11) Jung, B. J.; Tremblay, N. J.; Yeh, M.-L.; Katz, H. E. Molecular Design and Synthetic Approaches to Electron-Transporting Organic Transistor Semiconductors. *Chem. Mater.* **2010**, *23*, 568−582.
(12) Takacs, C. J.; Treat, N. D.; Krämer, S.; Chen, Z.; Facchetti, A.; Chabinyc, M. L.; Heeger, A. J. Remarkable Order of a High-Performance Polymer. *Nano Lett.* **2013**, *13*, 2522−2527.
(13) Lin, Y.; Fan, H.; Li, Y.; Zhan, X. Thiazole-Based Organic Semiconductors for Organic Electronics. *Adv. Mater.* **2012**, *24*, 3087−3106.
(14) Bronstein, H.; Chen, Z.; Ashraf, R. S.; Zhang, W.; Du, J.; Durrant, J. R.; Shakya Tuladhar, P.; Song, K.; Watkins, S. E.; Geerts, Y.; Wienk, M. M.; Janssen, R. A. J.; Anthopoulos, T.; Sirringhaus, H.; Heeney, M.; McCulloch, I. Thieno[3,2-*b*]thiophene−Diketopyrrolopyrrole-Containing Polymers for High-Performance Organic Field-Effect Transistors and Organic Photovoltaic Devices. *J. Am. Chem. Soc.* **2011**, *133*, 3272−3275.
(15) Park, Y. M.; Daniel, J.; Heeney, M.; Salleo, A. Room-Temperature Fabrication of Ultrathin Oxide Gate Dielectrics for Low-Voltage Operation of Organic Field-Effect Transistors. *Adv. Mater.* **2011**, *23*, 971−974.
(16) Xia, G.; Wang, S.; Zhao, X.; Zhou, L. High-Performance Low-Voltage Organic Transistor Memories with Room-Temperature

DOI: 10.1021/am507854s
ACS Appl. Mater. Interfaces 2015, 7, 2025−2031

Solution-Processed Hybrid Nanolayer Dielectrics. *J. Mater. Chem. C* **2013**, *1*, 3291−3296.
(17) Johnston, D. E.; Yager, K. G.; Nam, C.-Y.; Ocko, B. M.; Black, C. T. One-Volt Operation of High-Current Vertical Channel Polymer Semiconductor Field-Effect Transistors. *Nano Lett.* **2012**, *12*, 4181−4186.
(18) Kim, B. J.; Lee, S.-K.; Kang, M. S.; Ahn, J.-H.; Cho, J. H. Coplanar-Gate Transparent Graphene Transistors and Inverters on Plastic. *ACS Nano* **2012**, *6*, 8646−8651.
(19) Zhang, F.; Di, C. a.; Berdunov, N.; Hu, Y.; Hu, Y.; Gao, X.; Meng, Q.; Sirringhaus, H.; Zhu, D. Ultrathin Film Organic Transistors: Precise Control of Semiconductor Thickness Via Spin-Coating. *Adv. Mater.* **2013**, *25*, 1401−1407.
(20) Qi, Z.; Zhang, F.; Di, C.-a.; Wang, J.; Zhu, D. All-Brush-Painted Top-Gate Organic Thin-Film Transistors. *J. Mater. Chem. C* **2013**, *1*, 3072−3077.
(21) Diemer, P. J.; Lyle, C. R.; Mei, Y.; Sutton, C.; Payne, M. M.; Anthony, J. E.; Coropceanu, V.; Brédas, J. L.; Jurchescu, O. D. Vibration-Assisted Crystallization Improves Organic/Dielectric Interface in Organic Thin-Film Transistors. *Adv. Mater.* **2013**, *25*, 6956−6962.
(22) Wen, Y.; Liu, Y.; Guo, Y.; Yu, G.; Hu, W. Experimental Techniques for the Fabrication and Characterization of Organic Thin Films for Field-Effect Transistors. *Chemm. Rev.* **2011**, *111*, 3358−3406.
(23) Park, Y. D.; Park, J. K.; Lee, W. H.; Kang, B.; Cho, K.; Bazan, G. C. Post-Deposition Dipping Method for Improving the Electronic Properties of a Narrow Bandgap Conjugated Polymer. *J. Mater. Chem.* **2012**, *22*, 11462−11465.
(24) Dong, H.; Fu, X.; Liu, J.; Wang, Z.; Hu, W. 25th Anniversary Article: Key Points for High-Mobility Organic Field-Effect Transistors. *Adv. Mater.* **2013**, *25*, 6158−6183.
(25) Holliday, S.; Donaghey, J. E.; McCulloch, I. Advances in Charge Carrier Mobilities of Semiconducting Polymers Used in Organic Transistors. *Chem. Mater.* **2013**, *26*, 647−663.
(26) Yuan, Y.; Giri, G.; Ayzner, A. L.; Zoombelt, A. P.; Mannsfeld, S. C.; Chen, J.; Nordlund, D.; Toney, M. F.; Huang, J.; Bao, Z. Ultra-High Mobility Transparent Organic Thin Film Transistors Grown by an Off-Centre Spin-Coating Method. *Nat. Commun.* **2014**, *5*, 3005.
(27) Wang, H.; Yan, D. Organic Heterostructures in Organic Field-Effect Transistors. *NPG Asia Mater.* **2010**, *2*, 69−78.
(28) Chen, W.; Qi, D.; Gao, X.; Wee, A. T. S. Surface Transfer Doping of Semiconductors. *Prog. Surf. Sci.* **2009**, *84*, 279−321.
(29) Kim, J. H.; Yun, S. W.; An, B. K.; Han, Y. D.; Yoon, S. J.; Joo, J.; Park, S. Y. Remarkable Mobility Increase and Threshold Voltage Reduction in Organic Field-Effect Transistors by Overlaying Discontinuous Nano-Patches of Charge-Transfer Doping Layer on Top of Semiconducting Film. *Adv. Mater.* **2013**, *25*, 719−724.
(30) Cho, B.; Yu, S. H.; Kim, M.; Lee, M. H.; Huh, W.; Lee, J.; Kim, J.; Cho, J. H.; Lee, J. Y.; Song, Y. J. Discontinuous pn-Heterojunction for Organic Thin Film Transistors. *J. Phys. Chem. C* **2014**, *118*, 18146−18152.
(31) Lee, J.; Hwang, D.; Park, C.; Kim, S.; Im, S. Pentacene-Based Photodiode with Schottky Junction. *Thin Solid Films* **2004**, *451*, 12−15.
(32) Yoo, S.; Domercq, B.; Kippelen, B. Efficient Thin-Film Organic Solar Cells Based on Pentacene/C60 Heterojunctions. *Appl. Phys. Lett.* **2004**, *85*, 5427−5429.
(33) Hiroshiba, N.; Hayakawa, R.; Chikyow, T.; Yamashita, Y.; Yoshikawa, H.; Kobayashi, K.; Morimoto, K.; Matsuishi, K.; Wakayama, Y. Energy-Level Alignments and Photo-Induced Carrier Processes at the Heteromolecular Interface of Quaterrylene and *N,N′*-Dioctyl-3,4,9,10-perylenedicarboximide. *Phys. Chem. Chem. Phys.* **2011**, *13*, 6280−6285.
(34) Rahimi, R.; Roberts, A.; Narang, V.; Kumbham, V. K.; Korakakis, D. Study of the Effect of the Charge Transport Layer in the Electrical Characteristics of the Organic Photovoltaics. *Opt. Mater.* **2013**, *35*, 1077−1080.
(35) Krauss, T. N.; Barrena, E.; Zhang, X. N.; de Oteyza, D. G.; Major, J.; Dehm, V.; Würthner, F.; Cavalcanti, L. P.; Dosch, H. Three-Dimensional Molecular Packing of Thin Organic Films of PTCDI-C_8 Determined by Surface X-ray Diffraction. *Langmuir* **2008**, *24*, 12742−12744.
(36) Vasseur, K.; Rolin, C.; Vandezande, S.; Temst, K.; Froyen, L.; Heremans, P. A Growth and Morphology Study of Organic Vapor Phase Deposited Perylene Diimide Thin Films for Transistor Applications. *J. Phys. Chem. C* **2010**, *114*, 2730−2737.
(37) Lüssem, B.; Tietze, M. L.; Kleemann, H.; Hoßbach, C.; Bartha, J. W.; Zakhidov, A.; Leo, K. Doped Organic Transistors Operating in the Inversion and Depletion Regime. *Nat. Commun.* **2013**, *4*, 2775.
(38) Fiebig, M.; Beckmeier, D.; Nickel, B. Thickness-Dependent in Situ Studies of Trap States in Pentacene Thin Film Transistors. *Appl. Phys. Lett.* **2010**, *96*, 083304.
(39) Khim, D.; Baeg, K.-J.; Caironi, M.; Liu, C.; Xu, Y.; Kim, D.-Y.; Noh, Y.-Y. Control of Ambipolar and Unipolar Transport in Organic Transistors by Selective Inkjet-Printed Chemical Doping for High Performance Complementary Circuits. *Adv. Funct. Mater.* **2014**, *24*, 6252−6261.
(40) Le Comber, P.; Spear, W. Electronic Transport in Amorphous Silicon Films. *Phys. Rev. Lett.* **1970**, *25*, 509.
(41) Horowitz, G. Organic Field-Effect Transistors. *Adv. Mater.* **1998**, *10*, 365−377.
(42) Kang, H.; Lee, J.; Kim, M.; Joo, J.; Ko, J.; Lee, J. Electrical Characteristics of Pentacene-Based Thin Film Transistor with Conducting Poly(3,4-ethylenedioxythiophene) Electrodes. *J. Appl. Phys.* **2006**, *100*, 064508.
(43) Fritz, S. E.; Martin, S. M.; Frisbie, C. D.; Ward, M. D.; Toney, M. F. Structural Characterization of a Pentacene Monolayer on an Amorphous SiO_2 Substrate with Grazing Incidence X-ray Diffraction. *J. Am. Chem. Soc.* **2004**, *126*, 4084−4085.
(44) Ruiz, R.; Choudhary, D.; Nickel, B.; Toccoli, T.; Chang, K.-C.; Mayer, A. C.; Clancy, P.; Blakely, J. M.; Headrick, R. L.; Iannotta, S. Pentacene Thin Film Growth. *Chem. Mater.* **2004**, *16*, 4497−4508.
(45) Yang, H.; Kim, S. H.; Yang, L.; Yang, S. Y.; Park, C. E. Pentacene Nanostructures on Surface-Hydrophobicity-Controlled Polymer/SiO_2 Bilayer Gate-Dielectrics. *Adv. Mater.* **2007**, *19*, 2868−2872.
(46) Kim, S. H.; Jang, M.; Yang, H.; Park, C. E. Effect of Pentacene—Dielectric Affinity on Pentacene Thin Film Growth Morphology in Organic Field-Effect Transistors. *J. Mater. Chem.* **2010**, *20*, 5612−5620.
(47) Rivnay, J.; Steyrleuthner, R.; Jimison, L. H.; Casadei, A.; Chen, Z.; Toney, M. F.; Facchetti, A.; Neher, D.; Salleo, A. Drastic Control of Texture in a High Performance n-Type Polymeric Semiconductor and Implications for Charge Transport. *Macromolecules* **2011**, *44*, 5246−5255.

DOI: 10.1021/am507854s
ACS Appl. Mater. Interfaces 2015, 7, 2025−2031